

On Signal Processing and Testing Wave for Acoustic Gas Temperature and Flow Measurements[†]

Yukio FUKAYAMA^{*}, Nobuo MORIMOTO^{**}, Hiroshi KITAYAMA^{**},
Noriyuki IMADA^{**}, Katsumi SHIMOHIRA^{**} and Hitoshi OKIMURA^{**}

Optimal signal processing method and testing wave for acoustic gas thermometers and flow meters are discussed to improve their accuracy. The discussions are focused on time-of-flight shift type measurement using audio frequency region that are more suitable for hot, dusty or long distance acoustic paths than ultrasonic region. At first, matched filter with pre-whitener and their implementation with an AR (Autoregressive) model of noises are proposed for processing microphone received signal in order to identify the acoustic time-of-flight under noise contamination. Then, the PRK (phase reversal keying) of the M-sequence is shown to be proper for the testing wave that is sent into acoustic paths and improves the time-of-flight resolution. Finally, studies on practicality of the signal processing and the testing wave at thermal power stations as well as pilot plants are introduced.

1. INTRODUCTION

Acoustical non-contact methods have been required for gas thermometers and flow meters at furnaces, kilns, and large-scale ducts where the performances of conventional devices, thermo-couples, radiation thermometers, differential pressure flow meters etc., are limited by their dusty and high-temperature environments.

For examples, thermocouples are the typical contact method for conventional temperature measurements, but these sensors struggle with errors caused by radiation from the flames and with durability in furnaces where the gas temperature can reach up to 1400[°C]. Suction pyrometers, which divert the gas into measuring

sheaths and free the thermocouples from the radiation, should be considered only a temporary solution due to their frequent plugging. Radiation thermometers, the typical non-contact devices, also have a difficult time with distinguishing gas from flying dust and furnace walls. Moreover, large-scale ducts normally use a differential pressure type gas flow meters with either airfoils or orifices, however, the draft fan is known to cause a considerable loss of power. While the acoustical non-contact methods that apply sound time-of-flight to gas temperature and flow measurements hold the key to the solving foregoing performance limitation problems.

Fig.1 shows the acoustic gas temperature and flow measurement system that is investigated in this report. This system, which is called the time-of-flight shift type and is suitable for a wide range of measurements, consists of acoustic sensors that send and receive the sound. The sensors are connected to a testing wave generator and a signal processor. The signal processor identifies the time-of-flight, which is the traveling time of acoustical testing wave between the sensors. The time-of-flight measurement of the downstream and upstream are respectively abbreviated as τ_{BA} [s]

and τ_{AB} [s]. In addition, directions along with the known distance, L [m], and angle, θ [rad], can be used to calculate the flowing velocity, V_f [m/s], and the sound speed, V_s [m/s], as follows:

$$V_f = \frac{L}{2\cos\theta} \left(\frac{1}{\tau_{BA}} - \frac{1}{\tau_{AB}} \right) \quad (1),$$

$$V_s = \frac{L}{2} \left(\frac{1}{\tau_{BA}} + \frac{1}{\tau_{AB}} \right) \quad (2).$$

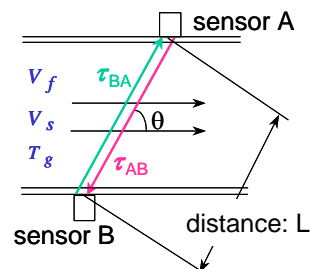


Fig.1 Temperature and flow measurement

Next, the gas temperature, T_g [°C], and mass flow, G [kg/s], can be calculated using the following equations based on the principle that the square of the sound speed is proportional to the absolute temperature:

$$T_g = 273.15 \left[\left(\frac{V_s}{V_{s0}} \right)^2 - 1 \right] \quad (3),$$

[†] Presented at '99 Kansai Chapter Symposium (1999•10)

^{*} Electronic Control Dept., Niihama National College of Tech., 7-1 Yakumo-cho, Niihama; Formerly Babcock-Hitachi Kure Research Lab.

^{**} Babcock-Hitachi Kure Research Lab. and Kure Division, 3-36 Takara-machi, Kure

$$G = AV_f \rho_0 \left(\frac{V_{s0}}{V_s} \right)^2 \quad (4).$$

In these equations, $A[\text{m}^2]$ denotes the gas flow cross-sectional area. Furthermore, $V_{s0}[\text{m/s}]$ and $\rho_0[\text{kg/m}^3]$, which should be obtained in advance, are the sound speed and the density of the gas at $0[\text{°C}]$ at the same pressure, respectively.

For the system shown in **Fig.1**, ultrasonic region that are typically used to improve the measurement accuracy should not be used for the acoustical testing wave. The waves should instead belong to the audio frequency region. This region accommodates long-distance acoustic paths in high-temperature and dusty environments. In addition, devices for audio frequency region are more economical. In order to obtain a sufficient time-of-flight measurement for τ_{BA} and τ_{AB} , which, as evident from Eqs. (1) and (2), dominate the measurement accuracy of the gas temperature and flow values, the signal processing method for the received signals as well as the testing wave sent into the objects should be studied under colored noise contamination that has originated from combustion, the Kalman vortex, and so on, which are typical in above mentioned plants and environments.

This report discusses the appropriate conditions of signal processing and testing wave for the acoustic gas temperature and flow measurements. Sections 2 and 3 present a method for detecting a known testing wave under contaminating colored noise and its implementation, respectively. Then, Sections 4 and 5 discuss the optimal testing wave and its implementation. Finally, Section 6 applies the proposed technique to practical gas temperature and flow measurements at pilot plants and a boiler. This research references a number of previous studies, such as the orthogonality application of the Walsh function by Tamura et al.^{13),14)}, studies on applying the chirp by Jitsumori et al.¹⁵⁾, as well as many fundamental studies by Thomas, Willet and others^{4),5)etc.}.

2. CONDITIONS FOR THE OPTIMAL SIGNAL PROCESSOR

In this research, the sought optimal signal processor is defined as the filter that provides the S/N maximum to the known testing wave before the threshold detector for identifying the time-of-flight. In early stages of this research, a type of cross-correlation method shown in Appendix A was applied to the signal processing. However, the method called matched filter in a narrow sense, did not prove to exhibit a sufficient performance under colored noise contamination, as presented in a previous report⁶⁾. Therefore, this section considers the affects of noise, and a S/N maximum filter equation that is based on a given testing wave, $\{s_k\}$ ($k = 0, 1, \dots, q$), and an auto-correlation, $r_N(n)$, of a noise sequence, $\{N_m\}$, is set up and solved. This procedure is resembling to the derivation of the Wiener filter⁴⁾.

At first, it is assumed that the signal, contaminated with noise,

reached the microphone at 0, for simplicity. The filter output of the signal, s_{oq} , and the noise, N_{oq} , at q are respectively described in terms of a filter impulse response, $\{h_k\}$ ($k = 0, 1, \dots, q$), as follows:

$$s_{oq} = \sum_{k=-\infty}^q h_{q-k} s_k = \sum_{k=0}^q h_{q-k} s_k \quad (5),$$

$$N_{oq} = \sum_{k=-\infty}^q h_{q-k} N_k \quad (6),$$

where the following zeros have supplied to the testing wave, $\{s_k\}$:

$$s_k = 0 \quad (k \leq -1, q+1 \leq k) \quad (7).$$

Therefore, the signal-to-noise ratio, $(S/N)_D$, at the destination, or at a threshold detector after the processor at q is derived as follows:

$$(S/N)_D = \frac{s_{oq}^2}{E\{N_{oq}^2\}} = \frac{\left(\sum_{k=0}^q s_k h_{q-k} \right)^2}{\sum_{k=-\infty}^q \sum_{j=-\infty}^q r_N(k-j) h_{q-j} h_{q-k}} \quad (8).$$

In this connection, $(S/N)_R$ denotes the signal-to-noise ratio at the receiving microphone, or before the processor.

Then, the sought filter equation with a maximum condition of $(S/N)_D$ in Eq. (8) is determined to be the following, by applying the variation technique presented in Appendix B^{1),4)}:

$$\sum_{m=0}^{\infty} r_N(n-m) h_m^o = s_{q-n} \quad (n = 0, 1, \dots) \quad (9),$$

where $\{h_n^o\}$ denotes the impulse response of the sought optimal filter.

Finally, the sought impulse response of the physically realizable (IUC) optimal filter can be obtained from $H^o(z)$, $S(z)$ and $\phi_N^+(z)$, which are the bilateral Z-transforms of $\{h_n^o\}$, $\{s_n\}$ and $r_N(n)$, respectively, as follows:

$$H^o(z) = \frac{1}{\phi_N^+(z)} \left[\frac{S(z^{-1})z^{-q}}{\phi_N^-(z)} \right]_+ = P(z) [P(z^{-1})S(z^{-1})z^{-q}]_+ \quad (10),$$

where, applying the spectral factorization technique presented in Appendix D^{1),4)}, $\phi_N^+(z)$ and $\phi_N^-(z)$ denote the IUC and OUC factors of power spectrum, $\phi_N(z)$, of $\{N_m\}$. In addition, the following pre-whitening filter, $P(z)$, described in Appendix C, is used:

$$P(z) = \frac{1}{\phi_N^+(z)} \quad (11)$$

Observing the left hand of Eq. (10), the sought filter consists of a tandem connection of $P(z)$ and a filter whose impulse response is the reverse order sequence of the q-step shifted output of the known testing wave, $\{s_k\}$, after passing through $P(z)$.

3. IMPLEMENTATION OF THE OPTIMAL SIGNAL PROCESSOR

In this section, an implementation of the signal processor described in the previous section shall be discussed. Fig.2 shows an example of the implementation in which contaminating colored noises are adaptively identified and pre-whitened.

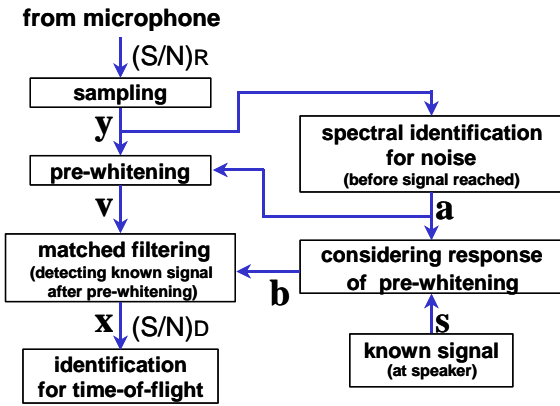


Fig.2 Processing flow for received signal

The IUC (inside the unit circle) factor, $\phi_N^+(z)$, of the noise power spectrum can be obtained from the coefficients in the AR (auto-regressive) model, and, for example, the RGI (recursive gradient identification) method is applicable as follows:

$$a_k^\# = a_{k-1}^\# + \frac{\rho}{k} (y_k - a_{k-1}^{\#T} y_k) y_k \quad (12)$$

where the following p -th order AR model coefficient, \mathbf{a} , and partial sequence vector, \mathbf{y}_k , of the microphone received sequence, $\{y_k\}$, are defined:

$$\mathbf{a} = (a_1 \ \dots \ a_p)^T, \ \mathbf{y}_k = (y_{k-1} \ \dots \ y_{k-p})^T \quad (13)$$

In addition, the superscript # and the subscript k indicate the k -th estimate calculated by the recursive estimation. Using RGI with a properly chosen positive constant, ρ , and an initial condition, $\mathbf{a}_0^\#$, the converged $\mathbf{a}^\#$ can be regarded as the true \mathbf{a} .

During the next step, the pre-whitening filter, $P(z)$, can be

obtained with the following pole-zero cancellation to $\phi_N^+(z)$:

$$P(z) = 1 - \sum_{m=1}^p a_m z^{-p} \quad (14)$$

Thus, the pre-whitened sequence $\{v_k\}$ can be obtained by the following FIR (finite impulse response) filter:

$$v_k = y_k - \mathbf{a}^T \mathbf{y}_k = (1 \ -a_1 \ \dots \ -a_p) \begin{pmatrix} y_k \\ \dots \\ y_{k-p} \end{pmatrix} \quad (15)$$

Next, the matched-filtered sequence, $\{x_k\}$, which prepares the processed signal vector, \mathbf{x} , for the threshold detector, is described as follows:

$$x_k = \mathbf{b}^T \mathbf{v}_k \quad (16)$$

where \mathbf{b} and \mathbf{v}_k respectively denote the following coefficient vector and pre-whitened sequence vector:

$$\mathbf{b} = (b_0 \ \dots \ b_q)^T, \ \mathbf{v}_k = (v_k \ \dots \ v_{k-q})^T \quad (17)$$

In this connection, each component of \mathbf{b} is matched with the testing wave after the whitening as follows:

$$b_{q-k} = s_k - \mathbf{a}^T \mathbf{s}_k \quad (18)$$

where \mathbf{s}_k denotes the following partial testing wave vector:

$$\mathbf{s}_k = (s_{k-1} \ \dots \ s_{k-p})^T \quad (19)$$

4. CONDITIONS FOR THE OPTIMAL TESTING WAVE

In the early stages of this research, a type of burst that requires more power to improve the $(S/N)_D$ was applied to the testing wave, but it was not able to provide a sufficient performance along long distance acoustic paths, as presented in a previous report^(6,7). Therefore, this section discusses an optimal testing wave with a unit signal power that further maximizes the $(S/N)_D$ of the optimal filter presented in the previous sections.

The optimal filter was developed for the maximum S/N conditions under a given testing wave $\{s_k\}$, ($k=0, \dots, q$) and noise auto-correlation $r_N(k)$ of the noise $\{N_m\}$. As mentioned in Appendix E, the $(S/N)_D$ of the optimal filter implementation in Section 3 can be described in the following matrix form:

$$(S/N)_D = \frac{s_{0q}^2}{E\{N_{0q}^2\}} = \mathbf{s}^* \mathbf{R}_N^{-1} \mathbf{s} \quad (20)$$

In this equation, the superscript * denotes the transpose of the complex conjugate and \mathbf{R}_N is in the Toeplitz form, which is described in Eq. (E-4) and is a positive definite matrix. In other

words, the matrix has positive eigenvalues $\{\lambda_0, \dots, \lambda_q\}$ and corresponding eigenvectors $\{e_0, \dots, e_q\}$ that constitute an orthonormal set. Thus, R_N can be expanded into the following outer product expansion:

$$R_N = \sum_{k=0}^q \lambda_k e_k e_k^* \quad (21).$$

Since the noise, $\{N_m\}$, can be modeled by the p -th order AR model, ($p \ll q$) and $r_N(k)$ s are practically zero in the over p region, the $(q+1)$ -length periodicity of $r_N(k)$ can be assumed. Thus, the discrete Fourier transform can be applied, and the concrete form of the eigenvectors are complex sinusoidal forms with angle frequencies, Ω_k ($k=0, \dots, q$), as follows:

$$e_k = \frac{1}{\sqrt{q+1}} (1 \quad \exp(j\Omega_k) \quad \dots \quad \exp(jq\Omega_k))^T \quad (22),$$

$$\Omega_k = \frac{2k\pi}{q+1} \quad (23),$$

where the eigenvalues with positive and symmetric properties are obtained from the following transformation:

$$\begin{pmatrix} \lambda_0 \\ \vdots \\ \lambda_q \end{pmatrix} = \begin{pmatrix} e_0^* \\ \vdots \\ e_q^* \end{pmatrix} \begin{pmatrix} r_N(0) \\ \vdots \\ r_N(q) \end{pmatrix} \quad (24),$$

$$\lambda_k = \lambda_{q+1-k} \geq 0 \quad (25).$$

Then, an arbitrary testing wave with a unit signal power can be expressed as the following form.

$$s = \sum_{k=0}^q c_k e_k \quad (26),$$

$$c_k = e_k^* s \quad (27),$$

where the expanding coefficients c_k ($k=0, \dots, q$) have the following constraint:

$$\sum_{k=0}^q |c_k|^2 = \sum_{k=0}^q c_k^* c_k = 1 \quad (28),$$

$$c_k^* = c_{q+1-k} \quad (29).$$

Therefore, Eq. (26) can be substituted into Eq. (20) due to the orthogonality of the eigenvectors. The lower bound of resulting S/N is evaluated as follows:

$$\begin{aligned} (S/N)_D &= \sum_{m=0}^q \sum_{n=0}^q \sum_{k=0}^q c_m^* e_m^* \lambda_n^{-1} e_n e_n^* c_k e_k \\ &= \sum_{k=0}^q \lambda_k^{-1} |c_k|^2 \geq (q+1) \left[\left(\prod_{k=0}^q \lambda_k^{-1} \right) \left(\prod_{k=0}^q |c_k|^2 \right) \right]^{\frac{1}{q+1}} \end{aligned} \quad (30),$$

where the theorems that state that the arithmetic mean of positive

numbers is not less than their geometrical mean, and that R_N^{-1} can be expanded in to the following form have been applied:

$$R_N^{-1} = \sum_{k=0}^q \lambda_k^{-1} e_k e_k^* \quad (31).$$

The optimal coefficients, c_k^o , in mini-max sense that maximizes the lower bound of $(S/N)_{D_{\max}}$ for all varying noise spectrum, λ_k , are obtainable using the Lagrange multiplier method explained in Appendix F as follows:

$$|c_k^o|^2 = \mathbf{arg\,max} \left\{ \prod_{k=0}^q |c_k|^2 \right\} = \frac{1}{q+1}, \quad (k=0, 1, \dots, q) \quad (32),$$

or the sought testing wave either has an identical power on each angle frequency ω_k , or it has auto-correlation similar to a white noise. Consequently, The optimal testing wave assures the following S/N at destination:

$$(S/N)_D = s^* R_N^{-1} s \geq \left(\prod_{k=0}^q \lambda_k^{-1} \right)^{\frac{1}{q+1}} \quad (33).$$

5. IMPLEMENTATION OF THE OPTIMAL TESTING SIGNAL

Since the pattern of the testing wave has to be known before received, M-sequence, a deterministic signal whose auto-correlation is sharp and nearly equal to that of the white noise, shall be investigated.

The L -th order M-sequence, $\{w_K\}$, ($K=0, \dots, N-1$; $N=2^L-1$) is recursively generated in the following manner:

$$w_K = a_0 w_{K-L} \oplus a_1 w_{K-L+1} \oplus \dots \oplus a_{L-1} w_{K-1}, \quad (K \geq L) \quad (34),$$

where an L -th order shift register with a proper initial value ($w_0, \dots, w_{L-1} = 0$ or 1) is chosen, and the \oplus operation denotes the exclusive-or. Furthermore, the coefficients, a_M ($M=0, \dots, L-1$), are those of the characteristic polynomial of order L 18):

$$z^L + a_{L-1} z^{L-1} + \dots + a_1 z + a_0 = 0 \quad (35).$$

Then, the binary sequence, $\{w_K\}$, is transmitted along acoustic paths via PRK (Phase Reversal Keying), shown in Fig.3, with the relationship between the carrier frequency, f_0 , and the chip width, d_c , established in order to allow $s(t)$ to be continuous. The sequence, $\{s_k\}$, is obtained through the Δt interval that samples l -times on the chip as follows:

$$s_k = s(k\Delta t) \quad \left(k=0, \dots, q; q=IN; \Delta t = \frac{d_c}{l} \right) \quad (36),$$

$$s(t) = p_L(t) \sin \omega_0 t \quad (37),$$

$$\omega_0 = 2\pi f_0 = \frac{2m\pi}{d_c} \quad \left(m = \frac{1}{2}, \frac{2}{2}, \frac{3}{2}, \dots \right) \quad (38),$$

where m , $p_L(t)$ and $\Pi(x)$ are the carrier cycles in the chip, the M-sequence pulse train, and the unit rectangular pulse, respectively. The rectangular pulse is defined as follows:

$$p_L(t) = \sum_{k=0}^{N-1} \left\{ (2w_k - 1) \Pi \left(\frac{t}{d_c} - K - \frac{1}{2} \right) \right\} \quad (39),$$

$$\Pi(x) = \begin{cases} 1, & (-\frac{1}{2} \leq x < \frac{1}{2}) \\ 0, & \text{(otherwise)} \end{cases} \quad (40).$$

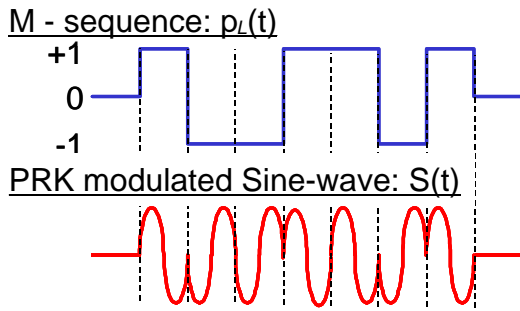


Fig.3 Testing signal for acoustic measurement

Furthermore, the carrier frequency, f_0 , should be chosen suitably for the frequency response of the acoustic path, since the power spectrum, $\Phi_s(\omega)$, of the testing wave has high density part around ω_0 and a band width of $(0, 2\omega_0)$, in case of $m=1$ in Eq. (39) as follows:

$$\begin{aligned} R_s(\tau) &= \frac{1}{Nd_c} \int_0^{Nd_c} s(t)s(t+\tau)dt \\ &= \frac{1}{2Nd_c} \int_0^{Nd_c} (\cos \omega_0 \tau - \cos(2\omega_0 t + \tau)) p_L(t) p_L(t+\tau) dt \\ &\approx \frac{1}{2} \cos \omega_0 \tau \int_0^{nd_c} p_L(t) p_L(t+\tau) dt \\ &\approx \frac{\exp(j\omega_0 \tau) + \exp(-j\omega_0 \tau)}{4} \Lambda \left(\frac{\tau}{d_c} \right) \\ \xleftrightarrow{\text{F.T.}} \Phi_s(\omega) &= \frac{d_c}{4} \left[\text{sinc}^2 \left(\frac{\omega + \omega_0}{\omega_c} \right) + \text{sinc}^2 \left(\frac{\omega - \omega_0}{\omega_c} \right) \right] \quad (41), \end{aligned}$$

where, $R_s(\tau)$ and $\xleftrightarrow{\text{F.T.}}$ denote the auto-correlation and the Fourier transform pair, respectively. The unit triangular pulse, $\Lambda(x)$, and the sinc function are defined as follows:

$$\Lambda(x) = \begin{cases} 1 - |x|, & (-1 \leq x < 1) \\ 0, & \text{(otherwise)} \end{cases} \quad (42),$$

$$\text{sinc}x \equiv \frac{\sin x}{x} \quad (43).$$

Fig.4 shows an FFT of an M-sequence PRK, $\{s_k\}$, with ($L=7$, $f_0=1/d_c=1$ [kHz]). This example demonstrates wide spectrum of $(0, 2f_0)$ that approximates that of white noises. The high power density part around f_0 is suitable for common audio devices. Performance comparisons between the optimal signal and the prior methods are summarized in another report¹⁾. This report states that in a typical case, containing a M-sequence PRK with ($L=4$, $f_0=5$ [kHz]) and speakers with a cut-off at 8[kHz], only a tenth of the burst signal in $(S/N)_R$ must be present at the microphone to keep the same $(S/N)_D$ at the threshold detector. Therefore, by applying the M-sequence PRK, the applicable furnace width is expected to increase by about three times for an acoustic gas measurement, which is inverse proportion of square root of the detectable $(S/N)_R$. In addition, its sharp signal after filtering decreases the chances of a detecting error, depending upon the threshold level used to identify the time-of-flight.

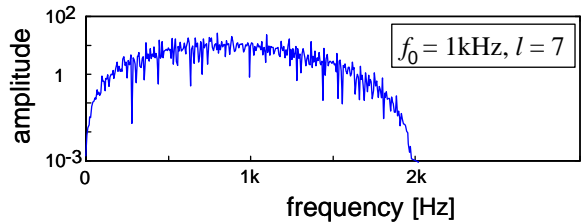


Fig.4 FFT of M-sequence PRK

6. ACTUAL EXAMPLES OF MEASUREMENTS

This section examines the performance and the practicality of the proposed processing method and testing wave in practical examples. The gas temperature and flow measurement results at the pilot plants and in a thermal power station boiler proved to be sufficient.

6.1 Temperature Measurement

The proposed acoustic thermometers were permanently installed in one of the largest capacity coal-fired boilers in Japan. The boiler, which is 30[m] wide and 80[m] tall, and generates 1000[MW] in electric power, has used these thermometers since July 1997. **Fig.5** shows a set of the sensors, which consists of twin

horns with a total of eight speakers and two microphones. The side wall of the boiler is equipped with lines of dust purging. The four sensor sets, which were installed on the front, rear, left and right side walls near the boiler furnace exit, provide six acoustic paths that transmit the testing wave around 1[kHz]. The acoustic thermometers have been utilized for adaptive control in the boiler for various types of coals for the five years period^{8),10)}.



Fig.5 Sensors on furnace wall

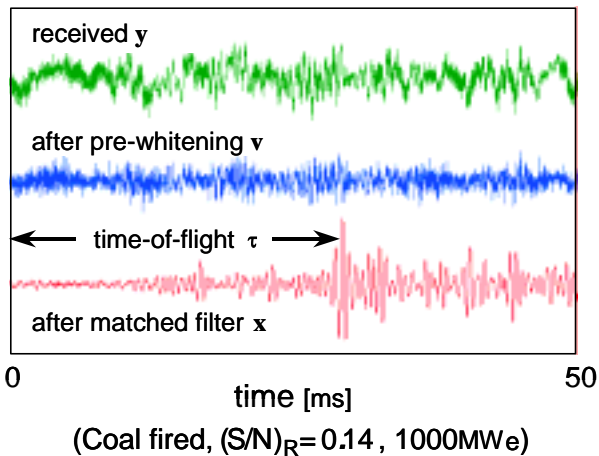


Fig.6 Processed signal with the M-sequence PRK

Fig.6 shows an example in the boiler under a considerably strong colored noise, estimated at $(S/N)_R=0.14$ before the processor. Although the received signals are severe, the processed signal, x , described in Fig.2 provides a clear peak for the time-of-flight identification with $(S/N)_D=5$ after the processor, which verifies the merit of the proposed technique. In addition, Fig.7 shows an example of the measurement during an emergency shut-down, which is often called a load rejection test, and the

re-start-up operation to full load, 1000[MW]. Although the state is changing rapidly, the measurement system is able to keep up with the transient gas temperature after the shutdown. In addition, the acoustic thermometers are also applied to cement kilns for quality control purposes¹²⁾.

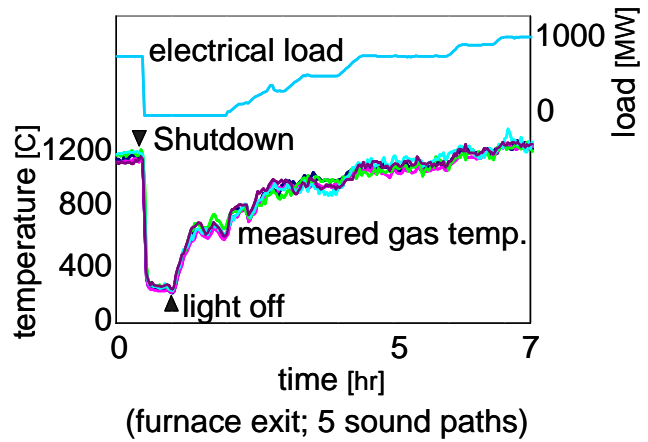


Fig.7 Temperature measurement at a 1000MWe boiler

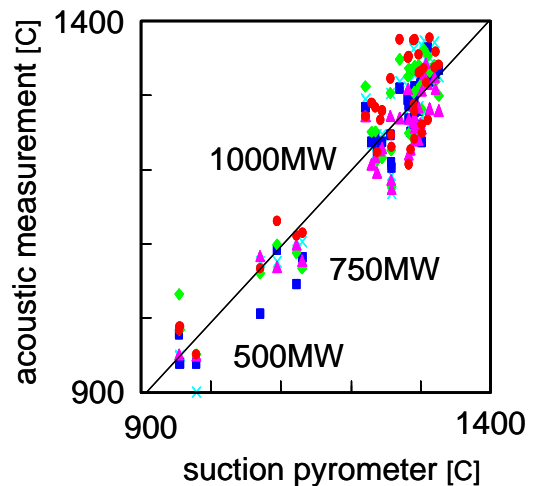


Fig.8 Result of temperature validation at the boiler

The acoustic temperature measurement in the boiler is validated in Fig.8 by comparing the readings with those from a suction pyrometer that was temporarily installed. The suction pyrometer consists of a thermocouple in a sheath and a gas ejector that prevents radiation errors. In this example, the acoustic measured values nearly coincide with those of the suction pyrometer, regardless of the type of coal or the load. The correlation between the two measurements is clear. Therefore, the acoustic measurement is shown to be a suitable replacement for suction pyrometers that experience a frequent plugging problem.

Furthermore, the accuracy of the acoustic temperature measurement has shown to provide more precise results in a laboratory pilot furnace measuring 2[m] in width and 10[m] in length. Fig.9 indicates that the difference between the acoustic measured values and the reference is due to the spatial average

from the five point thermocouple measurement shown in **Fig.10**. The standard deviation of the difference, in this example, is about three degrees, which is considered to be sufficient.

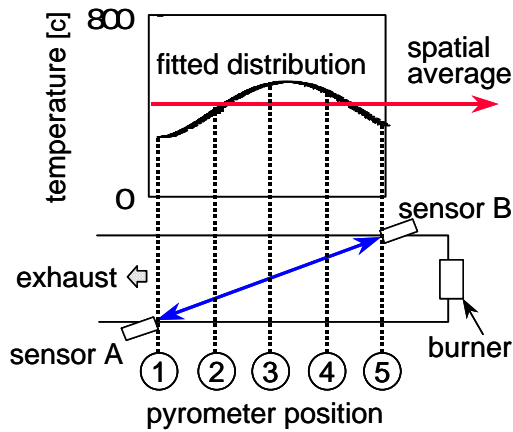


Fig.9 Gas temperature validation

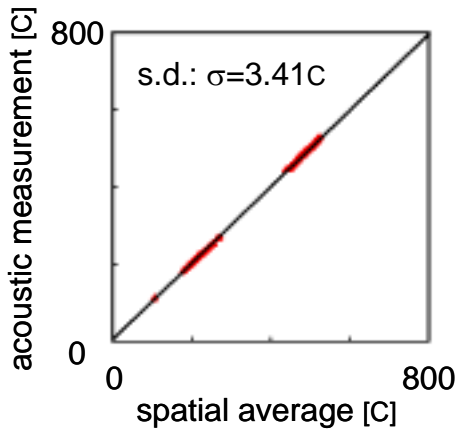


Fig.10 Result of temperature validation at a laboratory

6.2 Flow Measurement

The proposed signal processing method and testing wave, which is typically an M-sequence PRK transmitted around 10[kHz], have also been applied to acoustic gas flowmeters for large-scale ducts. This method has already been validated at a thermal power station boiler and a pilot plant, verifying its capability to follow state changes and measure velocity accurately.

Fig.11 shows a flow measurement comparison for a high gas temperature near 300[C] at a boiler duct measuring 3[m] square. The upper part of the figure indicates the results for the acoustic flow meter and the lower part are those for a conventional differential pressure type with air foils. The results suggest that the proposed system not only exhibits a sufficient capability in following the combustion and dumper opening pulses, but also demonstrates the same accuracy as the differential pressure measurement that is commonly used in boilers.

Furthermore, the acoustic flow meter was even more precise during a velocity swinging test in the range up to 30[m/s] in a

1[m] duct in the laboratory. **Fig.12** shows the relative deviation of the acoustic measurement from the linear resistance type and the difference pressure type flow meter references. In this experiment, the averages of measured values were taken every 20[cm] in depth on the duct with the linear resistance type flow meter. These results were used to verify the acoustic measurement in the low velocity region because the applicable turndown of the difference pressure type is known to be about one third of the maximum flow rate. When the linear resistance values were measured in the 10[m/s] region, the acoustic measurement agreed with the references within a 7[%] deviation in the range of 0[m/s] to 30[m/s]. Therefore, the acoustic flowmeter should be considered practical due to its sufficient accuracy over a wide range that includes nearly back flow status and without a draft loss.

These performance validation experiments have verified the adequacy of the proposed technique.

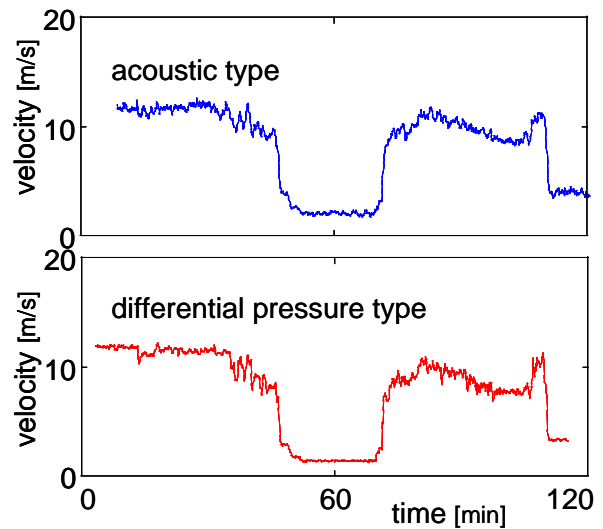


Fig.11 Flow measurement at a field duct

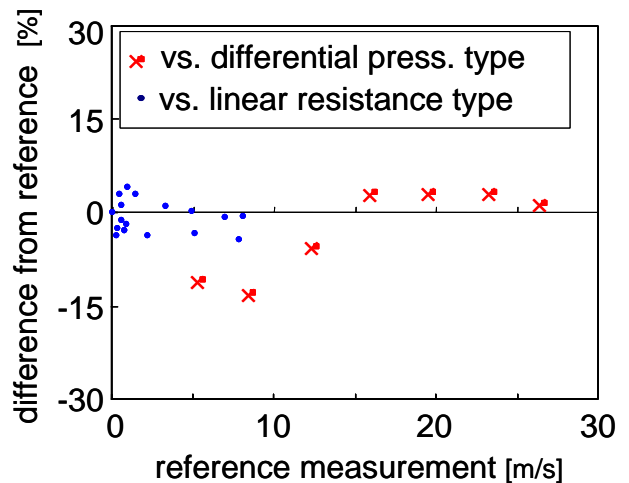


Fig.12 Result of flow validation at the duct

7. CONCLUSIONS

On signal processing and testing wave for acoustic gas temperature and flow measurement which is applying audio frequency region suitable for hot, dusty or long distance paths, the following studies have been pursued:

1. Conditions of signal processing method for identifying the time-of-flight under noise contamination were clarified; in addition, an implementation based on the Matched filter and the Pre-whitener which are successively renewed through an on-line spectral identification of contamination noises was proposed for the processing.
2. Conditions of acoustic testing signals for the path were clarified; in addition, the phase reverse keying of the M-sequence was proposed for the signal.
3. Sufficient performance and practicality of the processing method and the testing signal for the gas temperature and flow measurement were validated through results at pilot plants as well as a boiler of a thermal power station.

ACKNOWLEDGEMENTS

The authors would like to express profound thanks to the engineers at the Electric Power Development Co. Ltd. Matsuura Power Station in Nagasaki Japan for their advice and kind support. The Matsuura Power Station was the first plant that incorporated these techniques.

APPENDIX A. MATCHED FILTER IN NARROW SENSE

The sampled sequence of the known testing wave that is sent into the acoustic pats and the impulse response of the sought filter are denoted as $\{s_k\}$ and $\{h_k\}$, respectively. For simplicity, both of the lengths are the same, ($k=0,1,\dots,q$). Assuming that the signal reached the microphone at time 0 (in other words, the time-of-flight is 0), the output, x_q , of the sought filter at q can be expressed in terms of $\{h_k\}$ as:

$$x_q = \sum_{j=0}^q h_j s_{q-j} = \mathbf{h}^T \mathbf{s} \quad (\text{A-1}),$$

where the following vectors are defined for $\{h_k\}$ and the reverse order of $\{s_k\}$.

$$\mathbf{s} = (s_q \ \dots \ s_k \ \dots \ s_0)^T, \quad \mathbf{h} = (h_0 \ \dots \ h_k \ \dots \ h_q)^T \quad (\text{A-2}).$$

The maximum energy condition at q is used to identify the time-of-flight, assuming that the signal detection is reached at q steps before:

$$x_q^2 = (\mathbf{h}^T \mathbf{s})^2 \leq \|\mathbf{h}\|^2 \|\mathbf{s}\|^2 \quad (\text{A-3}),$$

where Schwarz's inequality holds with the condition in the parentheses, which is the maximum condition with an arbitrary constant κ . Thus, the following equality condition of Eq. (A-3) defines the matched filter in narrow sense, which is used in the context of not considering the noise:

$$\mathbf{h} = \kappa \mathbf{s} \quad (\text{A-4})$$

APPENDIX B. S/N MAXIMUM CONDITION ON FIR FILTER

Assuming that the maximum value of the S/N is α^{-1} , the following relationship is obtained from Eq. (8):

$$\sum_{k=-\infty}^q \sum_{j=-\infty}^q r_N(k-j) h_{q-j} h_{q-k} - \alpha \left(\sum_{k=0}^q s_k h_{q-k} \right)^2 = K \geq 0 \quad (\text{B-1}),$$

where K is at a minimum, the S/N maximum has been reached.

Next, the variation technique can be applied to Eq. (B-1), for obtaining the impulse response, $\{h_n^o\}$, of the optimal filter. Using an arbitrary variation, δh_n , and a constant, χ , any filter impulse response can be expressed as:

$$h_n = h_n^o + \chi \delta h_n \quad (\text{B-2}),$$

where the physically realizable condition, $h_n^o = 0$ at $n < 0$, holds.

In addition, since a scalar multiplication is not able to change the value of $(S/N)_D$ in Eq. (8), the amplitude of $\{h_n^o\}$ can be chosen to suffice the following constraint:

$$s_{0q}^o = \sum_{j=0}^q s_j h_{q-j}^o = \alpha^{-1} \quad (\text{B-3}),$$

where s_{0q}^o is the output of the known testing wave, $\{s_k\}$, through the sought filter.

Substituting Eq. (B-2) into Eq. (B-1). K is expressed as a function of χ , which includes the coefficients $K(0)$, A , and B , which are not dependent upon χ :

$$K(\chi) = K(0) + 2\chi A + \chi^2 B = B \left(\chi + \frac{A}{B} \right)^2 + K(0) - \frac{A^2}{B} \quad (\text{B-4}),$$

where A is expressed in the following concrete form:

$$A = \sum_{k=-\infty}^q \delta h_{q-k} \left[\sum_{j=-\infty}^q r_N(k-j) h_{q-j}^o - \alpha s_{0q}^o s_k \right] \quad (\text{B-5}).$$

The minimum of $K(\chi)$ has to occur at $\chi = 0$, A has to be zero for all arbitrary variations of δh_n . Thus, substituting Eq. (B-3) into the left hand of Eq.(B-5), the sought filter equation with the S/N maximum condition has been derived:

$$\sum_{m=0}^{\infty} r_N(n-m)h_m^o = s_{q-n} \quad (n=0,1,\dots) \quad (\text{B-6}),$$

where the subscripts, $q-j=m$ and $q-k=n$, were replaced.

APPENDIX C. WHITENING FILTER

A noise sequence, $\{N_m\}$, is treated as a set of random variables with w.s.s. (wide sense stationary) properties. Thus, the power spectrum, $\phi_N(z)$, and the auto-correlation of the noises are related by the following bilateral z-transform, $\mathbf{Z}\{\bullet\}$:

$$\phi_N = \mathbf{Z}\{r_N(n)\} = \sum_{n=-\infty}^{\infty} r_N(n)z^{-n} = [\phi_N(z)]_+ + [\phi_N(z)]_- \quad (\text{C-1}),$$

$$r_N(n) = \mathbf{E}\{N_m N_{m+n}\} = \mathbf{Z}^{-1}\{\phi_N(z)\} = \frac{1}{2\pi j} \oint_C \phi_N(z) z^{n-1} dz \quad (\text{C-2}),$$

where, the uni-lateral z-transform on the right side and the left side are described as follows, respectively:

$$[\phi_N(z)]_+ = \sum_{n=0}^{\infty} r_N(n)z^{-n}, \quad [\phi_N(z)]_- = \sum_{n=-\infty}^{-1} r_N(n)z^{-n} \quad (\text{C-3}).$$

Furthermore, when spectral factorization is applied, $\phi_N(z)$

becomes the product of ϕ_N^+ and ϕ_N^- , where the former contains all of the poles and zeros inside the unit circle (IUC) on the z-plane, and the latter contains those outside the circle (OUC):

$$\phi_N(z) = \phi_N^+(z)\phi_N^-(z) \quad (\text{C-4}).$$

Next, the inverse transforms of ϕ_N^+ and ϕ_N^- , respectively,

disappear on the left side and the right side in the time domain:

$$\frac{1}{2\pi j} \oint_C \phi_N^+(z) z^{n-1} dz = 0 \quad (n \geq 0) \quad (\text{C-5}),$$

$$\frac{1}{2\pi j} \oint_C \phi_N^-(z) z^{n-1} dz = 0 \quad (n < 0) \quad (\text{C-6}).$$

In addition, the following relationships are generated through spectral factorization:

$$\phi_N^+(z) = \phi_N^-(z^{-1}), \quad \phi_N^-(z) = \phi_N^+(z^{-1}) \quad (\text{C-7}).$$

Therefore, using the Wiener-Khinchine theorem, the whitening filter $P(z)$ for a noise sequence $\{N_m\}$ will satisfy the following equation⁴⁾:

$$\phi_N(z)P(z)P(z^{-1}) = \{\phi_N^+(z)P(z)\} \{\phi_N^-(z)P(z^{-1})\} = 1 \quad (\text{C-8}).$$

Thus, the physically realizable whitening filter, whose impulse response disappears on the left side, is obtained as follows:

$$P(z) = \frac{1}{\phi_N^+(z)} \quad (\text{C-9}).$$

APPENDIX D. SOLUTION OF THE OPTIMAL FILTER

Eq. (9) that the optimal filter must satisfy is solved with the spectral factorization. First, the following sequence, $\{g_n\}$, is defined:

$$g_n = s_{q-n} - \sum_{m=-\infty}^{\infty} r_N(n-m)h_m^o \quad (\text{D-1}),$$

where $g_n = 0$ at $n \geq 0$ is assumed.

Taking the bilateral z-transform of Eq. (D-1), the following OUC (outside the unit circle) function is obtained:

$$G(z) = S(z^{-1})z^{-q} - \phi_N(z)H^o(z) \quad (\text{D-2}),$$

where the notations are defined using the bilateral z-transform operator, $\mathbf{Z}\{\bullet\}$, as follows:

$$G(z) = \mathbf{Z}\{g_n\}, \quad S(z) = \mathbf{Z}\{s_n\}, \quad H^o(z) = \mathbf{Z}\{h_n^o\} \quad (\text{D-3}).$$

Applying the spectral factorization and the physically realizable condition, $h_n^o = 0$ at $n < 0$, Eq. (D-2) becomes a function whose left side and second term of the right side are OUC and IUC, respectively:

$$\frac{G(z)}{\phi_N^-(z)} = \frac{S(z^{-1})z^{-q}}{\phi_N^-(z)} - \phi_N^+(z)H^o(z) \quad (\text{D-4}).$$

Next, the inverse transform of terms in Eq. (D-4) are respectively defined as follows:

$$\xi_n = \mathbf{Z}^{-1}\left\{\frac{G(z)}{\phi_N^-(z)}\right\} \quad (\text{D-5}),$$

$$\eta_n = \mathbf{Z}^{-1}\left\{\frac{S(z^{-1})z^{-q}}{\phi_N^-(z)}\right\} \quad (\text{D-6}),$$

$$\zeta_n = \mathbf{Z}^{-1}\{\phi_N^+(z)H^o(z)\} \quad (\text{D-7}),$$

where, knowing the OUC and IUC properties, $\xi_n = 0$ at $n \geq 0$

and $\zeta_n = 0$ at $n < 0$ are to hold. In other words, the following relation is also available:

$$\zeta_n = \eta_n \quad (n \geq 0) \quad (\text{D-8}).$$

Therefore, knowing Eqs. (D-4) and (D-6), the bilateral z-transform of Eq. (D-8) can be written in the following form:

$$\mathbf{Z}\{\zeta_n\} = \phi_N^+(z)H^o(z) = [\phi_N^+(z)H^o(z)]_+ = \left[\frac{S(z^{-1})z^{-q}}{\phi_N^-(z)} \right]_+ \quad (\text{D-9}).$$

The sought impulse response of the physically realizable (IUC) optimal filter can now be obtained by dividing Eq. (D-9) by $\phi_N^+(z)$ as follows:

$$H^o(z) = \frac{1}{\phi_N^+(z)} \left[\frac{S(z^{-1})z^{-q}}{\phi_N^-(z)} \right]_+ = P(z) \left[\frac{S(z^{-1})z^{-q}}{\phi_N^-(z)} \right]_+ \quad (\text{D-10}).$$

APPENDIX E. MATRICES EXPRESSION OF S/N

Assuming that the testing wave reached the microphone at time 0, response of the testing wave, s_{0q} , and that of contaminating noise, N_{0q} , at time q through the optimal filter in Section 3 can respectively be expressed in the following matrix forms:

$$s_{0q} = \mathbf{s}^T \mathbf{U}^T \mathbf{U} \mathbf{s}, \quad N_{0q} = \mathbf{s}^T \mathbf{U}^T \mathbf{U} \mathbf{N}_q \quad (\text{E-1}),$$

where \mathbf{U} is the following $(q+1) \times (q+1)$ upper triangle matrix that includes the p -th order AR coefficients that satisfy $p \ll q$ condition:

$$\mathbf{U} = \begin{pmatrix} 1 & -a_1 & \cdots & -a_p & 0 & 0 & \cdots & 0 \\ 0 & 1 & -a_1 & \cdots & -a_p & 0 & \cdots & 0 \\ 0 & 0 & 1 & -a_1 & \cdots & -a_p & \cdots & 0 \\ \cdots & \cdots \\ 0 & 0 & 0 & 0 & 0 & 0 & \cdots & 1 \end{pmatrix} \quad (\text{E-2}).$$

In addition, the random variable vector, \mathbf{N}_m , contains partial sequence of the contaminating noise, $\{N_m\}$ with the w.s.s. assumption. This noise produces the auto-correlation matrix, \mathbf{R}_N , with the $(q+1) \times (q+1)$ Toeplitz form that does not depending on subscript m as follows:

$$\mathbf{N}_m = (N_m \quad N_{m-1} \quad \cdots \quad N_{m-q})^T \quad (\text{E-3}),$$

$$\mathbf{R}_N = \mathbf{E}\{\mathbf{N}_m \mathbf{N}_m^T\}$$

$$= \begin{pmatrix} r_N(0) & r_N(1) & \cdots & r_N(p) & \cdots & r_N(q) \\ r_N(1) & r_N(0) & \cdots & r_N(p-1) & \cdots & r_N(q-1) \\ \cdots & \cdots & \cdots & \cdots & \cdots & \cdots \\ r_N(p) & r_N(p-1) & \cdots & r_N(0) & \cdots & r_N(q-p) \\ \cdots & \cdots & \cdots & \cdots & \cdots & \cdots \\ r_N(q) & r_N(q-1) & \cdots & r_N(q-p) & \cdots & r_N(0) \end{pmatrix} \quad (\text{E-4}).$$

Since \mathbf{U} consists of the AR coefficients of $\{N_m\}$, the following relationship is applicable:

$$\mathbf{U} \mathbf{N}_m = \mathbf{W}_m \quad (\text{E-5}),$$

where \mathbf{W}_m denotes the partial sequence vector of the white noise:

$$\mathbf{W}_m = (W_m \quad W_{m-1} \quad \cdots \quad W_{m-q})^T \quad (\text{E-6}),$$

$$\mathbf{E}\{W_m W_n\} = \delta_{m,n} r_w \quad (\text{E-7}).$$

Taking the auto-correlation of Eq. (E-5), the following relationship can be derived:

$$\mathbf{R}_N^{-1} = \frac{1}{r_w} \mathbf{U}^T \mathbf{U} \quad (\text{E-8}).$$

Finally, substituting Eq. (E-1) and Eq. (E-8), the S/N at q can be obtained as follows:

$$(\text{S/N})_D = \frac{s_{0q}^2}{\mathbf{E}\{N_{0q}^2\}} = \frac{(\mathbf{s}^T \mathbf{R}_N^{-1} \mathbf{s})^2}{\mathbf{s}^T \mathbf{R}_N^{-1} \mathbf{E}\{N_q N_q^T\} \mathbf{R}_N^{-1} \mathbf{s}} \quad (\text{E-9}).$$

APPENDIX F: AN OPTIMAL CONDITION UNDER CONSTRAINT

In order to obtain the form of the maximum condition in Eq. (30) under the constraint in Eq. (28), the following Lagrangian function is considered:

$$L(|c_0|^2, \dots, |c_q|^2) = \prod_{k=0}^q |c_k|^2 + \mu \left(\sum_{k=0}^q |c_k|^2 - 1 \right) \quad (\text{F-1}),$$

where μ is a Lagrange multiplier.

Then, by differentiating Eq. (F-1) with respect to $|c_k|^2$ and setting the equation equal to zero, the sought coefficients are obtained:

$$|c_k|^2 = -\frac{\prod_{m=0}^q |c_m|^2}{\mu} = \frac{1}{q+1}, \quad (k=0, \dots, q) \quad (\text{F-2}).$$

REFERENCES

- 1) Y.Fukayama et al.: Acoustic Gas Temperature Measurement for Controlling Boilers Flexible with Fuels; Proc. of Japan/USA. Symposium on Flexible Automation, ASME, **10394A**, 433/440, Boston (1996)
- 2) G.Golub and C.Van Loan: Matrix Computations; John Hopkins University Press, London (1996)
- 3) N.Imada et al.: Measurement of Gas Temperature Distribution in Recovery Boilers Using Acoustic CT Method; Proc. of JSME-ASME Intl. Conf. on Power Engineering, **1**, 227/230, Tokyo (1993)
- 4) J.B.Thomas: An Introduction to Communication Theory and Systems; Springer-Verlag, New York (1988)
- 5) H.V.Van Trees: Detection, Estimation, and Modulation Theory; John Wiley & Sons, New York (1968)
- 6) Y.Fukayama and N.Imada: Applying the matched filtering to an acoustic gas temperature measurement at furnaces; Technical report IEICE, **EA94-58**, Hiroshima (1994)
- 7) Y.Fukayama and N.Imada: Study on the testing waves for acoustic gas temperature measurement; Proc. 4th Chugoku chapter conference of SICE, 248/249, Okayama (1995)
- 8) Y.Arai et al.: Development of adaptive controller for boilers firing various coals; Thermal and nuclear power, **47-11**, 1255/1262, Tokyo (1996)
- 9) Y.Fukayama and N.Imada: Temperature distribution measurement in boiler furnaces applying sound wave:

